Magnetoresistance Effects in the Metallic Antiferromagnet Mn_2Au

S. Yu. Bodnar,[1] Y. Skourski,[2] O. Gomonay,[1] J. Sinova,[1] M. Kläui,[1] and M. Jourdan[1,*]

[1] *Institut für Physik, Johannes Gutenberg-Universität, Staudingerweg 7, Mainz D-55099, Germany*

[2] *Hochfeld-Magnetlabor Dresden (HLD-EMFL), Helmholtz-Zentrum Dresden-Rossendorf, Dresden 01328, Germany*

(Received 27 September 2019; revised 15 May 2020; accepted 11 June 2020; published 1 July 2020)

In antiferromagnetic spintronics, it is essential to separate the resistance modifications of purely magnetic origin from other effects generated by current pulses intended to switch the Néel vector. We investigate the magnetoresistance effects resulting from magnetic-field-induced reorientations of the staggered magnetization of epitaxial antiferromagnetic $Mn_2Au(001)$ thin films. The samples are exposed to 60-T magnetic field pulses along different crystallographic in-plane directions of $Mn_2Au(001)$, while their resistance is measured. For the staggered magnetization aligned via a spin-flop transition parallel to the easy [110] direction, an anisotropic magnetoresistance of $\simeq -0.15\%$ is measured. In the case of a forced alignment of the staggered magnetization parallel to the hard [100] direction, evidence for a larger anisotropic magnetoresistance effect is found. Furthermore, transient resistance reductions of $\simeq 1\%$ are observed, which we associate with the annihilation of antiferromagnetic domain walls by the magnetic field pulses.

DOI: 10.1103/PhysRevApplied.14.014004

I. INTRODUCTION

In the emerging field of antiferromagnetic (AFM) spintronics [1–3], the orientation of the staggered magnetization, or more generally of the Néel vector, is used to encode information. Compared to conventional spintronics based on ferromagnets, antiferromagnets as active elements have the advantages of insensitivity to disturbing magnetic fields and intrinsic terahertz dynamics [4] potentially enabling ultrafast switching. For devices, the manipulation of the Néel vector by current-induced Néel spin-orbit torques (NSOTs) [5] is most promising and in principle the anisotropic magnetoresistance effect (AMR) can provide a readout mechanism. Thus, current-pulse-induced reversible resistance changes demonstrated for CuMnAs [6–8] and Mn_2Au [9–11] have been interpreted as originating from the AMR associated with the reorientation of the Néel vector.

Current-pulse-generated resistance switching has also been observed in polycrystalline metallic AFM MnN/Pt bilayers [12] and insulating AFM NiO/Pt bilayers [13–15] and is assumed to result from interfacial spin-orbit torques and spin Hall magnetoresistance for readout.

However, recently, similar current-pulse-induced resistance changes have been obtained investigating nonmagnetic cross structures consisting of pure Pt or Nb thin films. These experiments indicate that current-pulse-induced annealing could produce electrical signals similar to those observed in NiO/Pt [16,17]. For the intended advantages of antiferromagnetic spintronics, specifically concerning the ultrafast dynamics, it is essential that the Néel vector of the samples is manipulated and nothing else. Thus it is of major importance to investigate the obtainable magnetoresistance effects independent of current-pulse-based manipulation of the AFMs, i.e., to investigate resistance modifications purely associated with specific configurations of the Néel vector of antiferromagnetic domain configurations.

In this framework, we use a manipulation method of the Néel vector of Mn_2Au thin films, which guarantees that only magnetism-related properties of the AFM are affected, explicitly excluding all kinds of Joule-heating-related effects: Néel-vector reorientation by a large magnetic field pulse of up to 60 T. For a collinear AFM, it is energetically favorable if the magnetic moments are aligned perpendicular to the magnetic field, which allows them to cant slightly toward the field direction. This allows us to study the magnetoresistance effects originating from a reorientation of the Néel vector excluding all possible spurious effects. In general, one can consider three different magnetoresistance effects. First, there is the ordinary magnetoresistance (OMR), which appears in nonmagnetic metals as well. The field dependence of the OMR is nonhysteretic, depends on the details of the band structure, and is in general positive [18]. The longitudinal as well as the transversal OMR can amount to several percent for large

*jourdan@uni-mainz.de

fields (> 10 T) [19,20]. Second, there is the AMR, which, in AFM spintronics, is generally assumed to dominate the resistance modifications resulting from a current-induced reorientation of the Néel vector. Third, there is the domain-wall magnetoresistance (DWMR). This is a relevant effect in AFM spintronics, as the thin films are typically patterned into structures with lateral dimensions of several micrometers, whereas the typical AFM domain size is much smaller [21–24]. In ferromagnets, the transport of spin-polarized currents leads to scattering by the noncollinear spin structure imparted by domain walls [25,26]. Similar effects are possible for AFMs as well [27] but have been studied much less. One of the few AFM metals the domain-wall resistance of which has been experimentally investigated is Cr [28].

Here, we investigate the resistance changes induced by an reorientation of the Néel vector in epitaxial $Mn_2Au(001)$ thin films by a magnetic field pulse, i.e., we investigate pure magnetoresistance effects excluding heating effects. We focus on the hysteretic magnetoresistance associated with the DWMR and AMR, as we are interested in the switching effects of AFM spintronics.

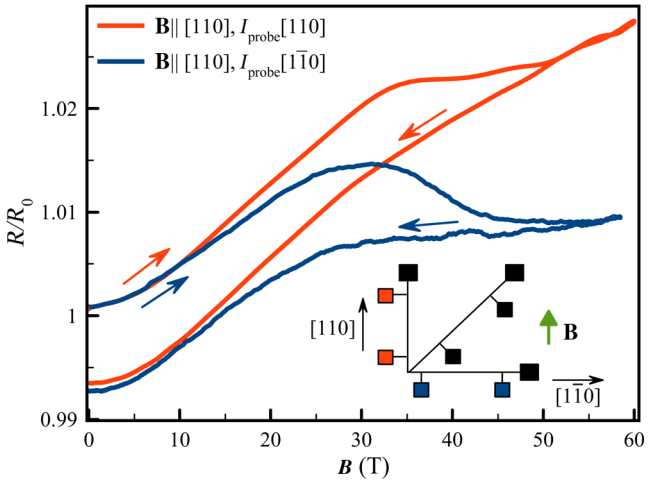

FIG. 1. The field-dependent resistances of a $Mn_2Au(001)$ epitaxial thin film measured during the exposure to magnetic field pulses along [110] with a duration of 150 ms, normalized to the sample resistances directly before the application of the respective field pulse. A waiting time of about 4 h is required between the two field pulses.

II. EXPERIMENTAL TECHNIQUES

For the electric transport measurements, an epitaxial $Mn_2Au(001)$ thin film with a thickness of 80 nm is deposited on a Al_2O_3 $(1\bar{1}02)$ substrate with a Ta(001) buffer layer (thickness 20 nm) as described in Ref. [29]. This sample is capped with 2 nm of Ta to prevent oxidation of the Mn_2Au surface and shows the same morphology as those investigated in Ref. [21]. For precise measurements of the resistance, it is patterned by optical lithography and ion-beam etching into three stripes of length 7 mm and width 200 μm, aligned parallel to the easy [110], easy [1$\bar{1}$0], and hard [100] directions of Mn_2Au, respectively. Separate contact pads at the ends of each stripe allow for four-probe measurements of the resistivity along the different crystallographic directions (see the inset of Fig. 1).

The sample is exposed to magnetic field pulses with an amplitude of 60 T and a pulse duration of 150 ms at the high-field laboratory of the Helmholtz Zentrum Dresden-Rossendorf (HLD-EMFL) to generate an alignment of the Néel vector perpendicular to the field direction. To ensure the stable temperature required for magnetoresistance measurements, the sample is immersed in liquid helium inside the cryostat within the field coil. During each pulse, and afterward for up to 10 s, the resistance R of one of the patterned Mn_2Au stripes is probed with a sampling rate of 200 kHz using a numerical lock-in technique with a probe current of 10^5 A/cm^2 modulated with a frequency of 20 kHz. In parallel, the magnetic field is obtained by numerical integration of the dB/dt signal induced in a pick-up coil situated next to the sample. This lock-in technique enables resistance measurements during the field-pulse application, while standard dc measurements are impossible due to the large induction effect generated by the magnetic field pulse. After each pulse, a waiting time of approximately 4 h is required for thermalization of the magnet coil, before the next pulse can be applied.

III. RESULTS

The magnetoresistance effects discussed below can only be understood if we first summarize our previous microscopic investigations of the persistent effects of large magnetic field pulses on the AFM domain pattern of our samples [21]. We show by x-ray magnetic linear dichroism−photoelectron emission microscopy (XMLD-PEEM) that the AFM domain pattern of as-grown $Mn_2Au(001)$ thin films consists of domains with an area of $\simeq 1$ μm^2, with the Néel vector aligned along both easy [110] and [1$\bar{1}$0] axes. Exposing the samples to a field pulse with an amplitude of $B_{pulse} = 30$ T along one easy axis results in a significantly increased area of AFM domains, with the Néel vector aligned perpendicular to the field pulse direction. The sample area covered by domains with this Néel-vector alignment is observed to saturate for $B_{pulse} =$ 50 T, i.e., an orientation of the Néel vector via spin-flop happens between 30 T and 50 T. We show that these domains with the Néel vector aligned perpendicular to the field-pulse direction are typically of slightly larger sizes than in the as-grown state of the samples and are separated by narrow wormlike spin structures with a width of $\simeq$ 100 nm (about twice the resolution limit of the PEEM). However, after the application of field pulses along the

hard [100] direction, we observe an equal part of the AFM domains with the Néel vector aligned parallel to both easy [110] and [1$\bar{1}$0] axes, with as well as slightly larger sizes than in the as-grown state [21].

From the resistance measurements presented here, we first discuss the effect of field pulses $\mathbf{B}(t)$ along an easy [110] direction of Mn_2Au, as this is associated with a straightforward modification of the magnetic state. The pulse generates a spin flop of all AFM domains with the Néel vectors $\mathbf{N} \parallel \mathbf{B}$, i.e., it results in a persistent alignment of $\mathbf{N} \perp \mathbf{B}$ as discussed above. This alignment results in a relatively small but persistent AMR effect, as we will discuss below. However, we first present the larger resistance modifications associated with the magnetic field pulse.

The red curve in Fig. 1 shows the resistance R of a $Mn_2Au(001)$ thin film (normalized to the resistance R_0 before the field pulse) probed along the easy [110] direction during a 150-ms pulse generating a time-dependent magnetic field $B(t)$ applied along the same direction.

Up to $B(t) \simeq 30$ T, $R(B)$ is governed by the nonhysteretic positive OMR. However, we focus on the hysteretic resistance modifications originating from the DWMR and AMR. Such effects appear above 30 T, which is exactly the magnetic field at which we have previously observed a spin-flop of most AFM domains with $\mathbf{N} \parallel \mathbf{B} \parallel [110]$. The hysteretic resistance reduction saturates at $\simeq 50$ T, which is the magnetic field at which the Néel vectors of all corresponding domains have completed the spin-flop alignment [21]. With a decreasing field below 30 T, $R(B)$ hysteretically reproduces the previous curve with a negative shift of the resistivity of $\simeq 0.75\%$, by which the sample resistivity directly after the pulse is reduced compared to its initial value.

As we will discuss below, this resistance reduction relaxes on a time scale of $\simeq 10$ s. So if the experiment is repeated some hours later with another field pulse, one starts with the same resistance that the as-grown sample had before the first field pulse plus a small AMR contribution, which we will discuss below. However, first we continue to discuss the relatively large resistance reduction, which appears at the spin-flop field of $\simeq 30$ T.

The blue curve in Fig. 1 shows R/R_0 of the same $Mn_2Au(001)$ thin film in a second field pulse along the same [110] direction 4 h later, but this time probed with contacts along the perpendicular [1$\bar{1}$0] direction: $R(B)$ shows a similar hysteresis as described above for the longitudinal resistance measurements, i.e., a reduction of the resistance at a magnetic field corresponding to the spin-flop field by a very similar value as discussed above for the probe current $\parallel$ [110].

For further investigation of the field-pulse-related resistance changes, the field is next applied along the hard [010] and [100] directions of the Mn_2Au thin films, while always probing with the current direction parallel to [010] (see the inset of Fig. 2). For these hard-axis directions of the magnetic field, no spin-flop is possible. Instead, the Néel vectors of the different AFM domains will rotate smoothly from the easy directions toward an alignment perpendicular to the field-pulse direction (hard axis), which they will reach at the spin-flop field. This means that a continuously growing contribution of the AMR effect to the total resistance change is expected for this field direction, which becomes zero again in zero field, with the Néel vector again aligned along the easy [110] and equivalent directions. Indeed, the dependence of the sample resistance on the current direction as shown in Fig. 2 is much stronger for the field along the hard [100] direction than for $\mathbf{B} \parallel [110]$. Although the directional dependence of the OMR, which also contributes, is unknown, this provides evidence for a large AMR in the order of some percent associated with the alignment of the Néel vector parallel to the hard [100] direction, in agreement with our previous calculations [9]. Additionally, also for the hard-axis field direction, a hysteretic resistance reduction is observed. It amounts to about 1.75%, which is about twice as large as for the easy-axis field direction.

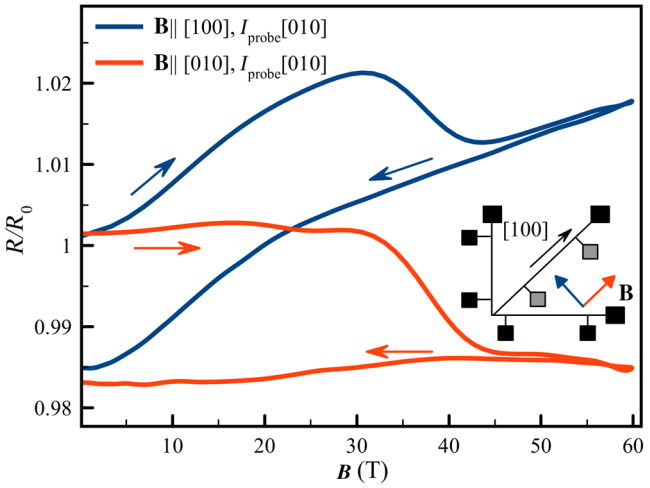

FIG. 2. The field-dependent resistances of a $Mn_2Au(001)$ epitaxial thin film measured during the exposure to magnetic field pulses along [010] and [100] with a duration of 150 ms, normalized to the sample resistances directly before the application of the respective field pulse. Note that between the two field pulses, the waiting time is about 4 h.

To understand the origin of these changes of the sample resistance, we next probe their temporal stability. These hysteretic resistance reductions are not persistent, i.e., they relax toward values relatively close to the original resistance of the sample before application of a field pulse: As shown in Fig. 3, the resistance reduction generated by the magnetic field exceeding the spin-flop field relaxes for pulses along the hard [010] as well as along the easy [110] direction of the $Mn_2Au(001)$ thin films on a time scale of 10 s. Its decay can be fitted by a logarithmic time dependence, which is typical for the relaxation of the

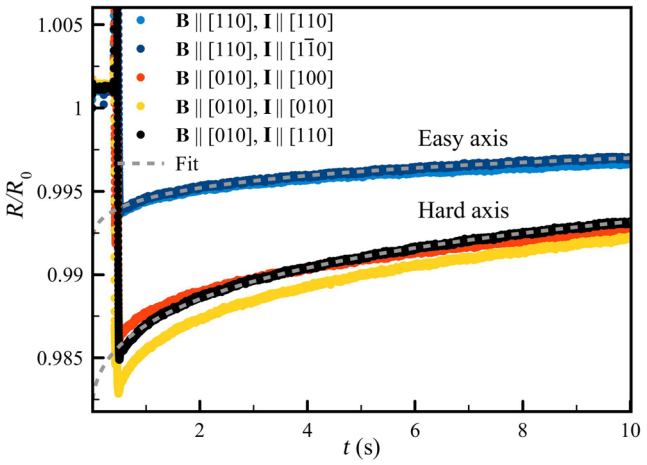

FIG. 3. The time dependence of the normalized resistances of a $Mn_2Au(001)$ epitaxial thin film probed along different current directions after the exposure to magnetic field pulses along the hard as well as along the easy in-plane axis. The resistance relaxes with a logarithmic time dependence as shown by the fits (dashed curves).

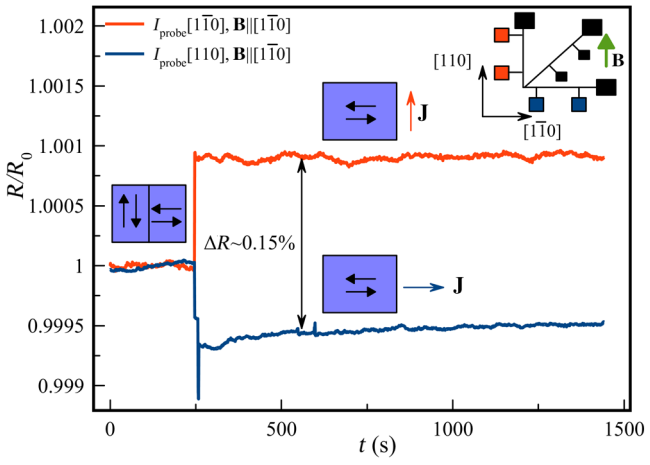

FIG. 4. The time-dependent resistance for different probe-current directions (see the inset) of a $Mn_2Au(001)$ thin film in the as-grown state and after the application of the first 60-T field pulse at $t \simeq 250$ s along the direction indicated in the inset. The standard dc measurement is unable to produce meaningful data for the first $\simeq 15$ s after the field pulse, due to overloading of the nanovoltmeter by the pulse-induced induction. The blue boxes indicate the alignment of the Néel vector.

magnetization of ferromagnets of different types [30,31]. Theoretically, this type of relaxation behavior was first associated with a flat-topped distribution of energy barriers [32], while it was later shown that it is rather universal for any distribution of energy barriers [33].

However, when checking the relaxation of the different signals, we find that not all resistance modifications associated with the field pulse are transient, as we discuss next.

After applying a field pulse along one of the easy-axis directions to a sample in the as-grown state, which consists of AFM domains with an equal distribution of domains with the Néel vector aligned along all four equivalent easy directions (see the images in Ref. [21]), the resistance does not relax completely to its original value. In Fig. 4, the time-dependent sample resistivity is shown for the first 20 min after application of a 60-T field pulse to an as-grown sample, measured by a standard dc measurement. Note that with this measurement technique, no meaningful data are obtained for the first $\simeq 15$ s after the field pulse, due to overloading of the dc nanovoltmeter by the pulse-induced induction. A persistent probe-current-direction-**J**-dependent increase and decrease of the sample resistance is observed (see the inset of Fig. 4). Correspondingly, if the resistance measurement shown in Fig. 2 is performed for the first time with a sample in the as-grown state and then 4 h later repeated with exactly the same configuration, the initial resistance is changed by exactly the value of the persistent resistance modification discussed here. This long-term persistent resistance change of $\Delta R \simeq -0.15\%$ is positive for a probe current parallel and negative for a probe current perpendicular to the field-pulse direction, which corresponds to an AMR effect. An AMR of similar size but with a different sign has recently been reported for CuMnAs [34].

IV. DISCUSSION AND CONCLUSIONS

We conclude that in Mn_2Au, there is a negative AMR of $\simeq -0.15\%$ at 4 K, associated directly with the spin-flop-driven Néel-vector reorientation. This experimentally observed AMR is in good agreement with our previously published calculations [9]: we consider the AMR of $Mn_2Au(001)$ theoretically for alignments of the Néel vector parallel to the [110] as well as parallel to the [100] direction. In the first case, we obtain $AMR_{[110]} \simeq -0.4\%$ and in the second case $AMR_{[100]} \simeq 6\%$. As we establish in the meantime, the [110] direction represents an easy axis within the easy (001)-plane [21]; thus the calculation is in good agreement with the experimental results shown in Fig. 4. Furthermore, as already discussed above, the previously calculated $AMR_{[110]}$ of the order of several percent is also consistent with the experimentally observed anisotropy of the resistance with the Néel vector forced by the field pulse to align along the hard axis (Fig. 2).

However, AMR cannot account for the field-pulse-generated hysteretic transient resistance reductions, which appear for all field directions at the spin-flop field. This effect can be explained based on the DWMR. Independent of the physical mechanism of the DWMR, the large magnetic field during the pulse makes any alignment of the Néel vector parallel to the field energetically unfavorable. Thus it is likely that during a field pulse with a magnitude

above the spin-flop field, all domain walls are removed. However, we know from the XMLD-PEEM investigation of our samples performed weeks after the field pulses that even in samples with a persistent spin-flop-induced reorientation of the Néel vector, domain walls exist. We also know that in all configurations the field pulses reduce the resistance of the Mn_2Au thin films at the spin-flop field, followed by an increase of the resistance after the pulse. Thus we can consistently assume that the domain walls produce a significant DWMR, which is identified by removing the domain walls during the field pulse. After the pulse, on the time scale of 10 s (at 4 K) given by the measured relaxation time of the resistance, the domain walls reform. As the density of the domain walls is very similar in the as grown and in the field manipulated samples [21], the contribution of the DWMR to the sample resistance before and after the field pulse is also very similar. A microscopy-based verification of this model is highly desired but unfortunately is not possible, as XMLD-PEEM imaging of the domain of Mn_2Au cannot be realized on the time scale of 1 s after a 50-T field pulse. Furthermore, we can only speculate about the physical origin of the relatively large DWMR, which is implied by our analysis: we propose that it is related to the specific anisotropies in the band structure of Mn_2Au, from which the large calculated $AMR_{[100]} \simeq 6\%$ [9] also originates. In a domain wall, the Néel vector is pointing along the hard [100] direction as well and confinement effects could further increase its magnitude.

Finally, we relate the magnetoresistance effects and magnetic anisotropies discussed here to our previous observation of reversible current-pulse-induced resistance changes of up to 6% [9]: those large effects were obtained for current pulses along the—as we now know, magnetically hard—[100] direction and they were much larger than the persistent $AMR_{[110]} \simeq -0.15\%$ determined experimentally here. Thus we can now exclude the AMR of AFM domains with the Néel vector aligned by current pulses as the origin of these large resistance modifications. However, here we provide evidence for a potentially large DWMR in Mn_2Au, which could well explain the observed resistance changes in the current pulse experiments. Clearly, this requires further investigations combining the microscopic observation of current-induced AFM-domain manipulation with *in situ* resistance measurements.

V. SUMMARY

In summary, we identify the magnitude of the AMR $\simeq -0.15\%$ in Mn_2Au associated with the persistent alignment of the Néel vector along the magnetic easy [110] axis. Forcing the Néel vector to align parallel to the hard [100] axis, we provide experimental evidence for an AMR of several percent for this orientation of the staggered magnetization. These experimental values are consistent with our previous calculations of the AMR [9]. Furthermore, we observe field-pulse-induced transient resistance reductions of $\simeq 1\%$, which are consistent with the assumption of removal and subsequent reformation of AFM domain walls. This model implies a relatively large domain-wall magnetoresistance in Mn_2Au. Such large domain wall resistances would provide opportunities in antiferromagnetic spintronics such as racetrack memory [35] or multilevel switching [36] and could explain the large resistance changes generated by current pulses applied to our $Mn_2Au(001)$ thin films [9].

ACKNOWLEDGMENTS

This work was funded by the Deutsche Forschungsgemeinschaft (DFG, German Research Foundation) Grant No. TRR 173 268565370 (projects A01, A03, A05, and B12). We acknowledge the support of the HLD at the Helmholtz-Zentrum Dresden-Rossendorf, a member of the European Magnetic Field Laboratory (EMFL).

[1] T. Jungwirth, J. Sinova, A. Manchon, X. Marti, J. Wunderlich, and C. Felser, The multiple directions of antiferromagnetic spintronics, Nat. Phys. **14**, 200 (2018).

[2] V. Baltz, A. Manchon, M. Tsoi, T. Moriyama, T. Ono, and Y. Tserkovnyak, Antiferromagnetic spintronics, Rev. Mod. Phys. **90**, 015005 (2018).

[3] M. B. Jungfleisch, W. Zhang, and A. Hoffmann, Perspectives of antiferromagnetic spintronics, Phys. Lett. A **382**, 865 (2018).

[4] T. Kampfrath, A. Sell, G. Klatt, A. Pashkin, S. Mähllein, T. Dekorsy, M. Wolf, M. Fiebig, A. Leitenstorfer, and R. Huber, Coherent terahertz control of antiferromagnetic spin waves, Nat. Phot. **5**, 31 (2011).

[5] J. Železný, H. Gao, K. Výborný, J. Zemen, J. Mašek, A. Manchon, J. Wunderlich, J. Sinova, and T. Jungwirth, Relativistic Néel-Order Fields Induced by Electrical Current in Antiferromagnets, Phys. Rev. Lett. **113**, 157201 (2014).

[6] P. Wadley, B. Howells1,J. Železný, C. Andrews, V. Hills, R. P. Campion, V. Novák, K. Olejník, F. Maccherozzi, S. S. Dhesi, *et al.*, Electrical switching of an antiferromagnet, Science **351**, 587 (2016).

[7] J. Godinho, H. Reichlová, D. Kriegner, V. Novák, K. Olejník, Z. Kašpar, Z. Šobáň, P. Wadley, R. P. Campion, R. M. Otxoa, *et al.*, Electrically induced and detected Néel vector reversal in a collinear antiferromagnet, Nat. Commun. **9**, 4686 (2018).

[8] T. Matalla-Wagner, M.-F. Rath, D. Graulich, J.-M. Schmalhorst, G. Reiss, and M. Meinert, Electrical Néel-Order Switching in Magnetron-Sputtered CuMnAs Thin Films, Phys. Rev. Appl. **12**, 064003 (2019).

[9] S. Yu. Bodnar, L. Šmejkal, I. Turek, T. Jungwirth, O. Gomonay, J. Sinova, A. A. Sapozhnik, H.-J. Elmers, M. Kläui, and M. Jourdan, Writing and reading antiferromagnetic Mn_2Au by Néel spin-orbit torques and

large anisotropic magnetoresistance, Nat. Commun. **9**, 348 (2018).
[10] X. F. Zhou, J. Zhang, F. Li, X. Z. Chen, G. Y. Shi, Y. Z. Tan, Y. D. Gu, M. S. Saleem, H. Q. Wu, F. Pan, *et al.*, Strong Orientation-Dependent Spin-Orbit Torque in Thin Films of the Antiferromagnet Mn_2Au, Phys. Rev. Appl. **9**, 054028 (2018).
[11] M. Meinert, D. Graulich, and T. Matalla-Wagner, Electrical Switching of Antiferromagnetic Mn_2Au and the Role of Thermal Activation, Phys. Rev. Appl. **9**, 064040 (2018).
[12] M. Dunz, T. Matalla-Wagner, and M. Meinert, Spin-orbit torque induced electrical switching of antiferromagnetic MnN, Phys. Rev. Res. **2**, 013347 (2020).
[13] X. Z. Chen, R. Zarzuela, J. Zhang, C. Song, X. F. Zhou, G. Y. Shi, F. Li, H. A. Zhou, W. J. Jiang, F. Pan, *et al.*, Antidamping-Torque-Induced Switching in Biaxial Antiferromagnetic Insulators, Phys. Rev. Lett. **120**, 207204 (2018).
[14] T. Moriyama, K. Oda, T. Ohkochi, M. Kimata, and T. Ono, Spin torque control of antiferromagnetic moments in NiO, Sci. Rep. **8**, 14167 (2018).
[15] L. Baldrati, O. Gomonay, A. Ross, M. Filianina, R. Lebrun, R. Ramos, C. Leveille, F. Fuhrmann, T. R. Forrest, and F. Maccherozzi, *et al.*, Mechanism of Néel Order Switching in Antiferromagnetic Thin Films Revealed by Magnetotransport and Direct Imaging, Phys. Rev. Lett. **123**, 177201 (2019).
[16] C. C. Chiang, S. Y. Huang, D. Qu, P. H. Wu, and C. L. Chien, Absence of Evidence of Electrical Switching of the Antiferromagnetic Néel Vector, Phys. Rev. Lett. **123**, 227203 (2019).
[17] T. Matalla-Wagner, J.-M. Schmalhorst, G. Reiss, N. Tamura, and M. Meinert, Resistive contribution in electrical switching experiments with antiferromagnets, arXiv:1910.08576 (2019).
[18] J. Callaway, *Quantum Theory of the Solid State* (Academic Press, London, 1991).
[19] B. Lüthi, Longitudinal Magnetoresistance of Metals in High Fields, Phys. Rev. Lett. **2**, 503 (1959).
[20] A. B. Pippard, *Magnetoresistance in Metals* (Cambridge University Press, Cambridge, 1989).
[21] A. A. Sapozhnik, M. Filianina, S. Yu. Bodnar, A. Lamirand, M.-A. Mawass, Y. Skourski, H.-J. Elmers, H. Zabel, M. Kläui, and M. Jourdan, Direct imaging of antiferromagnetic domains in Mn_2Au manipulated by high magnetic fields, Phys. Rev. B **97**, 134429 (2018).
[22] M. J. Grzybowski, P. Wadley, K. W. Edmonds, R. Beardsley, V. Hills, R. P. Campion, B. L. Gallagher, J. S. Chauhan, V. Novak, and T. Jungwirth, *et al.*, Imaging Current-Induced Switching of Antiferromagnetic Domains in CuMnAs, Phys. Rev. Lett. **118**, 057701 (2017).
[23] P. Wadley, S. Reimers, M. J. Grzybowski, C. Andrews, M. Wang, J. S. Chauhan, B. L. Gallagher, R. P. Campion, K. W. Edmonds, S. S. Dhesi, *et al.*, Current polarity-dependent manipulation of antiferromagnetic domains, Nat. Nanotech. **13**, 362 (2018).
[24] S. Yu. Bodnar, M. Filianina, S. P. Bommanaboyena, T. Forrest, F. Maccherozzi, A. A. Sapozhnik, Y. Skourski, M. Kläui, and M. Jourdan, Imaging of current induced Néel vector switching in antiferromagnetic Mn_2Au, Phys. Rev. B **99**, 140409(R) (2019).
[25] C. H. Marrows, Spin-polarised currents and magnetic domain walls, Adv. Phys. **54**, 585 (2005).
[26] A. von Bieren, A. K. Patra, S. Krzyk, J. Rhensius, R. M. Reeve, L. J. Heyderman, R. Hoffmann-Vogel, and M. Kläui, Domain-Wall Induced Large Magnetoresistance Effects at Zero Applied Field in Ballistic Nanocontacts, Phys. Rev. Lett. **110**, 067203 (2013).
[27] J.-H. Zheng A. Brataas, M. Kläui, and A. Qaiumzadeh, Domain-Wall Magnetoresistance in Antiferromagnetic Metals, arXiv:2004.07154 (2020).
[28] R. Jaramillo, T. F. Rosenbaum, E. D. Isaacs, O. G. Shpyrko, P. G. Evans, G. Aeppli, and Z. Cai, Microscopic and Macroscopic Signatures of Antiferromagnetic Domain Walls, Phys. Rev. Lett. **98**, 117206 (2007).
[29] M. Jourdan, H. Braeuning, A. A. Sapozhnik, H. J. Elmers, H. Zabel, and M. Kläui, Epitaxial Mn_2Au thin films for antiferromagnetic spintronics, J. Phys. D: Appl. Phys. **48**, 385001 (2015).
[30] R. Street and J. C. Wooley, A study of magnetic viscosity, Proc. Phys. Soc. London A **62**, 562 (1949).
[31] Y. Liu, D. J. Sellmyer, and D. Shindo, *Handbook of Advanced Magnetic Materials: Vol. 1 Nanostructural Effects* (Springer Science & Business Media, Berlin, 2008).
[32] S.-K. Ma, Dynamics of a vector spin-glass model, Phys. Rev. B **22**, 4484 (1980).
[33] J. M. González-Miranda and J. Tejada, Computer-simulation study of magnetic relaxation in anisotropic magnetic systems, Phys. Rev. B **49**, 3867 (1994).
[34] M. Wang, C. Andrews, S. Reimers, O. J. Amin, P. Wadley, R. P. Campion, S. F. Poole, J. Felton, K. W. Edmonds, and B. L. Gallagher, *et al.*, Spin flop and crystalline anisotropic magnetoresistance in CuMnAs, Phys. Rev. B **101**, 094429 (2020).
[35] S.-H. Yang, K.-S. Ryu, and S. Parkin, Domain-wall velocities of up to 750 m/s driven by exchange-coupling torque in synthetic antiferromagnets, Nat. Nanotech. **10**, 221 (2015).
[36] K. Olejník, V. Schuler, X. Marti, V. Novák, Z. Kašpar, P Wadley, R. P. Campion, K. W. Edmonds, B. L. Gallagher, J. Garces, *et al.*, Antiferromagnetic CuMnAs multilevel memory cell with microelectronic compatibility, Nat. Commun. **8**, 15434 (2017).